AGU PUBLICATIONS

Global Biogeochemical Cycles

RESEARCH ARTICLE
10.1002/2015GB005257

Key Points:
- Uncertainty over source of CO_2 during the end of the Little Ice Age (LIA)
- ^{14}C-dated Southern Hemisphere tree rings provide measure of ocean ventilation
- Southern Ocean upwelling suppressed suggesting a terrestrial source for CO_2

Correspondence to:
C. S. M. Turney,
c.turney@unsw.edu.au

Citation:
Turney, C. S. M., et al. (2016), Multidecadal variations in Southern Hemisphere atmospheric ^{14}C: Evidence against a Southern Ocean sink at the end of the Little Ice Age CO_2 anomaly, *Global Biogeochem. Cycles*, *30*, doi:10.1002/2015GB005257.

Received 29 JUL 2015
Accepted 15 JAN 2016
Accepted article online 18 JAN 2016

Multidecadal variations in Southern Hemisphere atmospheric ^{14}C: Evidence against a Southern Ocean sink at the end of the Little Ice Age CO_2 anomaly

Chris S. M. Turney[1], Jonathan Palmer[1], Alan Hogg[2], Christopher J. Fogwill[1], Richard T. Jones[3], Christopher Bronk Ramsey[4], Pavla Fenwick[5], Pauline Grierson[6], Janet Wilmshurst[7,8], Alison O'Donnell[6], Zoë A. Thomas[1], and Mathew Lipson[1]

[1]Climate Change Research Centre and School of Biological, Earth and Environmental Sciences, University of New South Wales, Sydney, New South Wales, Australia, [2]Waikato Radiocarbon Laboratory, University of Waikato, Hamilton, New Zealand, [3]Department of Geography, Exeter University, Devon, UK, [4]Research Laboratory for Archaeology and the History of Art, University of Oxford, Oxford, UK, [5]Gondwana Tree-Ring Laboratory, Canterbury, New Zealand, [6]Ecosystems Research Group, School of Plant Biology, University of Western Australia, Crawley, Western Australia, Australia, [7]Landcare Research, Lincoln, New Zealand, [8]School of Environment, University of Auckland, Auckland, New Zealand

Abstract Northern Hemisphere-wide cooling during the Little Ice Age (LIA; 1650–1775 Common Era, C.E.) was associated with a ~5 ppmv decrease in atmospheric carbon dioxide. Changes in terrestrial and ocean carbon reservoirs have been postulated as possible drivers of this relatively large shift in atmospheric CO_2, potentially providing insights into the mechanisms and sensitivity of the global carbon cycle. Here we report decadally resolved radiocarbon (^{14}C) levels in a network of tree-ring series spanning 1700–1950 C.E. located along the northern boundary of, and within, the Southern Ocean. We observe regional dilutions in atmospheric radiocarbon (relative to the Northern Hemisphere) associated with upwelling of $^{14}CO_2$-depleted abyssal waters. We find the interhemispheric ^{14}C offset approaches zero during increasing global atmospheric CO_2 at the end of the LIA, with reduced ventilation in the Southern Ocean and a Northern Hemisphere source of old carbon (most probably originating from deep Arctic peat layers). The coincidence of the atmospheric CO_2 increase and reduction in the interhemispheric ^{14}C offset imply a common climate control. Possible mechanisms of synchronous change in the high latitudes of both hemispheres are discussed.

1. Introduction

Climate-carbon feedbacks are potentially a significant source of future warming [*Cox et al*., 2000; *Friedlingstein et al*., 2013; *Gregory et al*., 2009; *Meinshausen et al*., 2011], driven by changes in the natural sinks and sources of greenhouse gases [*Collins et al*., 2013]. A major source of uncertainty is the oceanic response to future forcing [*Friedlingstein et al*., 2013; *Le Quéré et al*., 2009, 2007; *Séférian et al*., 2012]. In the oceans, the dominant carbon sink today is widely considered to be the Southern Ocean [*Bernardello et al*., 2014; *Le Quéré et al*., 2007], but the dearth of continuous observations prior to the late twentieth century limits our understanding of regional contributions, how these may have changed over time, and the mechanisms of change [*Friedlingstein et al*., 2013; *Landschützer et al*., 2015; *Le Quéré et al*., 2009].

A potential way of extending historical observations of Southern Ocean air-sea carbon fluxes is the exploitation of atmospheric radiocarbon (^{14}C). Here deep water formation in the North Atlantic isolates surface water as part of the Meridional Overturning Circulation, most of which upwells in the Southern Ocean, induced by the strong, persistent westerly winds in the Southern Hemisphere [*Marshall and Speer*, 2012]. The slow pace of deep ocean circulation allows a sufficient amount of radioactive decay to significantly reduce radiocarbon activity of the abyssal waters, resulting in the upwelling (and outgassing) of "old" CO_2 on seasonal through to millennial timescales [*Braziunas et al*., 1995; *Galbraith et al*., 2011; *Hogg et al*., 2013], depleting Southern Hemisphere atmospheric ^{14}C levels with a postulated change of 1‰ (8 ^{14}C years) per 10° of latitude [*Braziunas et al*., 1995]. While the longest observational record of atmospheric $^{14}CO_2$ is available from 1954 Common Era (C.E.) (Wellington, New Zealand) [*Currie et al*., 2011], annually resolved records of tree growth have a proven ability to preserve a passive measure of changing atmospheric radiocarbon, potentially reaching back millennia [*Turney and Palmer*, 2007].

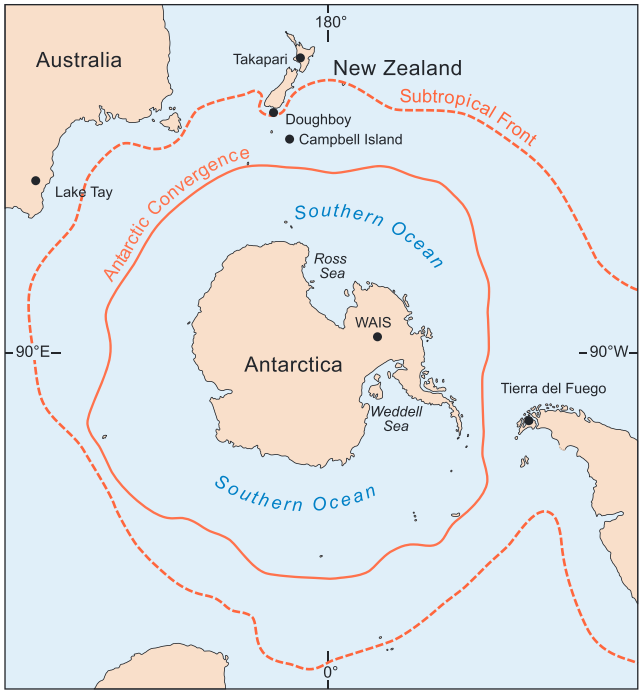

Figure 1. Location of tree ring ^{14}C series discussed in text, the West Antarctic Ice Sheet (WAIS) Divide ice core [*Bauska et al.*, 2015], and mean locations of the Subtropical and Polar fronts (red lines).

A period of particular interest for understanding past climate-carbon interactions is 1650 to 1775 C.E., during which time atmospheric CO_2 appears to have been ~5 ppmv below pre 1650 C.E. levels [*Ahn et al.*, 2012; *Cox and Jones*, 2008; *Etheridge et al.*, 1996; *Rubino et al.*, 2013]. This slightly lower CO_2 appears associated with maximum cooling within a multicentennial Northern Hemisphere-wide climatic downturn commonly described as the "Little Ice Age" (LIA; 1250–1850 C.E.) [*Mann et al.*, 2009; *PAGES 2 k Consortium*, 2013]. The decrease and subsequent increase in atmospheric CO_2 provides a useful constraint on the century timescale sensitivity of the carbon cycle to climate change [*Cox and Jones*, 2008]. While early observations raised the possibility that the Southern Ocean may have been a driver behind these changes in atmospheric CO_2 [*Trudinger et al.*, 1999], recent work has suggested instead that Northern Hemisphere terrestrial sources were the primary cause, through either land use changes [*Kaplan*, 2015] or the vulnerability of deep Arctic peat layers to decay with warming toward the end of the LIA [*Bauska et al.*, 2015].

Here we investigate changes in the circulation of the Southern Ocean using decadally resolved atmospheric radiocarbon levels within tree rings across the midlatitudes of the Southern Hemisphere. Using ^{14}C as a proxy of upwelling, we test whether the Southern Ocean played a significant role in climate-carbon dynamics during the end of the LIA chronozone.

2. Methods

We collected wood samples for tree ring analysis at their southernmost growing limit along the northern fringes of, and within, the Southern Ocean: (1) *Callitris columellaris* from Lake Tay, Western Australia (33.03°S, 120.75°E) [*Cullen and Grierson*, 2009]; (2) *Libocedrus bidwillii* from Takapari Forest Park, North Island, New Zealand (40.07°S, 175.98°E) [*Hogg et al.*, 2002]; (3) *Halocarpus biformis* from Doughboy Bay, Stewart Island, New Zealand (47.47°S, 167.73°E); and (4) *Dracophyllum longifolium* from Northeast Harbour, Campbell Island, New Zealand (52.52°S, 169.22°E) (Figure 1). Each tree series formed part of a well-replicated, annually resolved chronology with an "expressed population signal" (or EPS) above 0.85, a threshold value commonly used to describe a robust, highly replicated series [*Briffa and Jones*, 1990]. The Northeast Harbour *Dracophyllum longifolium* series did not extend all the way to 1700 C.E. and was only sampled to 1900 C.E. Supplementing these series are the reported radiocarbon measurements obtained from *Nothofagus dombeyi* in Tierra del Fuego, southern Chile (54°S, 71°W) [*McCormac et al.*, 2002; *Stuiver and Braziunas*, 1998], from which decadally averaged means were calculated up to 1850 C.E. (Table 1).

The tree ring series were decadally sampled from 1700 C.E. (to capture the latter part of the LIA chronozone) up to 1950 C.E. (immediately prior to the bomb spike) [*Hua et al.*, 2013]. A cross section (or biscuit) was cut and transported to the laboratory where a radial strip was removed for analysis and the residual offcuts archived. The radial strip was first dried and then sanded progressively stepping from coarse to fine grit paper until a highly polished surface was obtained. After this step, the radii were studied under a binocular microscope, and the annual rings cross dated and assigned a calendar year. Growths rings were then grouped according

Table 1. Decadal Radiocarbon (^{14}C) Ages for Southern Hemisphere Tree Ring Series[a]

Years (C.E.)	Lake Tay (Wk-)	Lake Tay ($^{14}C \pm 1\sigma$)	Takapari (Wk-)	Takapari ($^{14}C \pm 1\sigma$	Doughboy (Wk-)	Doughboy ($^{14}C \pm 1\sigma$)	Campbell Island (Wk-)	Campbell Island ($^{14}C \pm 1\sigma$)	Tierra del Fuego ($^{14}C \pm 1\sigma$)[c]
1705	39,764	188 ± 26	39,564	132 ± 23	39,540	167 ± 22			153 ± 3
1715	39,765	172 ± 23	39,565	165 ± 23	39,541	167 ± 24			139 ± 3
1725	39,766	177 ± 23	39,566	170 ± 22	39,542	210 ± 23			165 ± 7
1735	39,767	227 ± 23	39,567	188 ± 24	39,543	199 ± 26			202 ± 10
1745	39,768	232 ± 26	39,568	204 ± 24	39,544	250 ± 24			215 ± 10
1755	39,769	240 ± 23	39,569	233 ± 23	39,545	246 ± 22			213 ± 10
1765	39,770	220 ± 23	39,570	217 ± 23	39,546	217 ± 22			224 ± 10
1775	39,771	234 ± 22	39,571	212 ± 23	39,547	208 ± 25			214 ± 5
1785	39,772	249 ± 16	39,572	249 ± 15	39,548	225 ± 19			226 ± 6
1795	39,773	242 ± 19	39,573	203 ± 13	39,549	197 ± 13			230 ± 6
1805	39,587	205 ± 22	39,574	193 ± 23	39,550	185 ± 22			176 ± 5
1815	39,588	173 ± 24	39,575	141 ± 22	39,551	148 ± 22			133 ± 5
1825	39,589	169 ± 22	39,576	136 ± 22	39,552	154 ± 25			105 ± 10
1835	39,590	163 ± 22	39,577	180 ± 23	39,553	161 ± 24			148 ± 8
1845	39,591	148 ± 20	39,578	147 ± 21	39,554	157 ± 20			166 ± 8
1855	39,592	142 ± 20	39,579	112 ± 20	39,555	157 ± 19			
1865	39,593	140 ± 22	39,580	128 ± 21	39,556	124 ± 21			
1875	39,594	126 ± 23	39,581	140 ± 20	39,557	162 ± 20			
1885	39,595	132 ± 22	39,582	166 ± 19	39,558	141 ± 20			
1895	39,596	114 ± 20	39,583	117 ± 20	39,559	127 ± 19			
1905	39,597	106 ± 21	39,584	117 ± 20	39,560	130 ± 21	39,602	138 ± 22	
1915	39,598, 41,047[b]	130 ± 14	39,585	104 ± 13	41,046[b]	139 ± 24	39,603	140 ± 20	
1925	41,049[b]	153 ± 20	39,586	140 ± 21	39,562, 41,048[b]	148 ± 14	39,604	167 ± 22	
1935	39,600, 41,051[b]	168 ± 15	40,118	166 ± 21	41,050[b]	177 ± 20	39,605	170 ± 22	
1945	41,053[b]	164 ± 20	40,119	187 ± 13	41,052[b]	155 ± 20	39,606	211 ± 12	

[a]Years given as the midpoint of the dated decadal block. University of Waikato laboratory numbers are denoted by "Wk-".
[b]Multiple samples used to calculate a weighted mean and age uncertainty.
[c]Radiocarbon data set previously reported for Tierra del Fuego [*McCormac et al.*, 2002; *Stuiver and Braziunas*, 1998]; multiple ages within each decade have been used to derive a weighted mean and age uncertainty.

to decade (e.g., 1940–1949 and 1930–1939) and bulk decadal samples collected by separating each decade of rings along a ring boundary by first making fine radial cuts with a band saw and then using a chisel. As such, the internal age incorporation for each sample is 10 years. For radiocarbon (^{14}C) dating, chemical pretreatment of the bulked (decadal) wood samples resulted in the purification of alpha-cellulose as this wood fraction is deemed the most reliable for minimizing potential contamination and providing the most robust ^{14}C ages required for such high-precision study [*Hogg et al.*, 2006]. Alpha-cellulose extraction begins with an acid-base-acid pretreatment at 80°C, with samples treated with 1 N HCl for 60 min, followed by successive 30 min treatments with 1 N NaOH until the supernatant liquid remained clear, ending with another 60 min 1 N HCl wash. Holocellulose was then extracted by using successive 30 min treatments of acidified $NaClO_2$ at 70°C until the wood shavings were bleached to a pale yellow color. Alpha-cellulose was then prepared by a final treatment with NaOH followed by a further acid wash (1 N HCl at 70°C for 30 min), and repeated washing with distilled water until a pH of >6 was achieved. Samples were then graphitised in the Waikato Radiocarbon Laboratory and measured for radiocarbon by accelerator mass spectrometry at the University of California at Irvine (UCI). For the youngest samples (i.e., 1940–1950) an initial solvent extraction was added to remove mobile components (resins, etc.) thereby reducing the potential for "bomb" ^{14}C translocating across the ring boundaries. A major advantage of all samples being prepared in one laboratory (Waikato) and measured for ^{14}C in a single facility (UCI) is the potential for interlaboratory inconsistencies to be avoided, reducing the age uncertainties (Table 1).

Radiocarbon ages of the samples were compared to the Northern Hemisphere radiocarbon data set (IntCal13) [*Reimer et al.*, 2013] using a Defined Sequence model (`D_Sequence`) [*Bronk Ramsey and Lee*, 2013] in OxCal 4.2. To accommodate the mean Southern Hemispheric offset, a `Delta_R` with the prior U(−10, 90) was used (allowing a 50 year or 0.625% margin either side of 40 years or 0.5%). Using Bayes theorem, the algorithms employed sample possible solutions with a probability that is the product of the prior and likelihood probabilities. Taking into account the age model and the actual ^{14}C age measurements, the posterior probability densities quantify the most likely age distributions and allowed us to estimate

Table 2. Calculated Regional Radiocarbon (^{14}C Years $\pm 1\sigma$) Offsets Across Common Periods

Time Period	Lake Tay (Western Australia), 33°S	Takapari (North Island NZ), 40°S	Dough Boy (Stewart Island), 47°S	Campbell Island (Southern Ocean), 53°S	Tierra del Fuego (S. America), 54°S
1700–1850	57.0 ± 6.0	37.7 ± 5.7	44.4 ± 5.9		38.0 ± 2.6
1850–1950	17.5 ± 6.5	15.3 ± 6.2	25.0 ± 6.6	30.2 ± 9.3	
1700–1950	39.0 ± 4.4	26.7 ± 4.2	35.0 ± 4.4		

regional offsets to the Northern Hemisphere across common periods of time. To determine a time series of changing regional offsets to the Northern Hemisphere, the IntCal13 data set was extracted at 0.5 year intervals from OxCal 4.2 and the mean decadal difference with weighted error calculated (Table 2). We then compared the weighted mean and standard deviations of both the IntCal13 and our Southern Hemisphere series using a *t* test of each pair of values at each decade. This was done to determine time periods when no significant difference occurred (i.e., no interhemispheric offset).

3. Results and Discussion

The new Southern Hemisphere tree ring ^{14}C series record large offsets from the average Northern Hemisphere radiocarbon data set IntCal13 [*Reimer et al.*, 2013]. For the common period of overlap (1700–1850 C.E.), the Takapari (North Island) ^{14}C measurements are statistically identical to the previously reported New Zealand Takapari-Hihitari ages produced by the University of Waikato (-3 ± 29 years) [*Hogg et al.*, 2002] providing confidence that the data set is comparable to SHCal13 [*Hogg et al.*, 2013] but offering greater sample depth over the last 300 years. Dividing the tree sequences into preindustrial and postindustrial periods, the larger offsets were recorded prior to 1850 C.E. at Lake Tay in Western Australia (57.0 ± 6.0 ^{14}C years) and Doughboy (Stewart Island; 44.4 ± 5.9 ^{14}C years) (Table 2); the smaller offsets were recorded at Takapari and Tierra del Fuego (southern Chile) at 37.7 ± 5.7 and 38 ± 2.6 ^{14}C years, respectively. With industrialization, we observe a decrease in the offset, with Lake Tay (17.5 ± 6.5 ^{14}C years), Takapari (15.3 ± 6.2 ^{14}C years), and Doughboy (25.0 ± 6.6 ^{14}C years) all recording a marked decline after 1850 C.E. In the time period captured by Northeast Harbour, Campbell Island (1900–1950 C.E.), the subantarctic series preserves the greatest offset to IntCal13, with a difference of 30.2 ± 9.3 ^{14}C years.

Two important points can be made from the above observations. First, there is no obvious Southern Hemisphere latitudinal ^{14}C gradient [*Braziunas et al.*, 1995]. While Campbell Island (53°S) exhibits the largest of all the ^{14}C offsets from the Northern Hemisphere, Tierra del Fuego, which is at a similar high-latitude (54°S) shows one of the smallest offsets and Lake Tay, which is at a much lower latitude (33°S) shows relatively old ages. Second, regional offsets in Southern Hemisphere atmospheric radiocarbon are measureable, though whether this is due to differences in the growing seasons (as suggested for the Northern Hemisphere) [*Bronk Ramsey et al.*, 2010; *Manning et al.*, 2001] is presently unclear. We therefore concentrate on the temporal variations preserved across the data sets.

Previous work has indicated that temporal variability in Southern Hemisphere atmospheric $^{14}CO_2$ is strongly influenced by sea ice extent in the Southern Ocean but with the potential for regional differences [*Braziunas et al.*, 1995]. To investigate multidecadal to centennial changes in the atmospheric radiocarbon offset, we compare the mean of Southern Hemisphere ^{14}C ages with the IntCal13 Northern Hemisphere record [*Reimer et al.*, 2013] (Figure 2). Although the long-term trend is most probably a result of industrialization and a greater emission of fossil fuels (dead ^{14}C) in the Northern Hemisphere from 1850 C.E. [*Ahn et al.*, 2012; *McCormac et al.*, 1998], at least two prominent reductions in the offsets appear to be recorded; a *t test* between the data points of the two series shown in Figure 2 identified the periods 1780–1800 C.E., 1860–1870, and possibly post 1930 (Figures 2 and 3; gray shaded columns). Similar periods when the offset converged on zero have also been suggested for New Zealand during 1725–1795 C.E. and 1805–1865 [*McCormac et al.*, 1998], the timing of which is consistent with our wider Southern Hemisphere results. The sustained nature of these multidecadal fluctuations in the tree ring series suggests a natural, time-varying component in the atmospheric ^{14}C content may be operating in the Southern Hemisphere.

To explore the observed changes in more detail (independent of differences in the growing season across the network of sites), we generated individual time series of the mean decadal difference (offset) to IntCal13 for

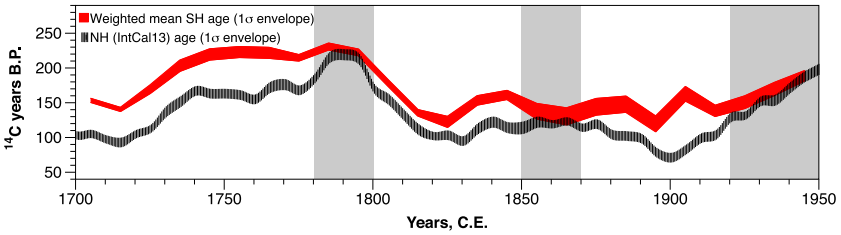

Figure 2. Weighted mean Southern Hemisphere atmospheric ^{14}C age (red envelope; 1σ range) compared to the Northern Hemisphere IntCal13 data set (dashed black envelope; 1σ range) [*Reimer et al.*, 2013]. Gray columns denote periods discussed in text.

each record (Figure 3). Offsets are observed among the different ^{14}C data sets, but importantly there is a remarkable degree of coherence in temporal variability between the different sites (Figure 3), implying changes in the flux of old carbon to the atmosphere. Fitting a locally weighted smoothing (LOESS) curve to the individual series identifies a long-term trend toward a negligible offset between our study regions and IntCal13 [*Reimer et al.*, 2013]. The greatest change is observed at Lake Tay where the offset declines from a maximum value of ~83 ^{14}C years (1700–1710 C.E.) to ~28 ^{14}C years across 1790–1800 C.E.

Importantly, the collapses in ^{14}C offset to the Northern Hemisphere centered on 1790 and 1860 C.E. are observed in all our records, indicating that the shifts were Southern Hemisphere-wide and not region-specific. The ~60 year recurrence interval of interhemispheric collapse may be linked to the 120–130 year periodicity in UK-NZ ^{14}C differences [*Hogg et al.*, 2011] suggested to be driven by changes in sea ice extent and wind speed [*Braziunas et al.*, 1995] or as recent studies have proposed, changes in the latitude of core flow [*Rodgers et al.*, 2011] over the Southern Ocean. A poleward shift in westerly airflow over the Southern Hemisphere has been found to enhance northward Ekman transport of cool Antarctic surface waters, drawing up more carbon-rich (^{14}C-depleted) subsurface waters south of the Antarctic Circumpolar Current [*Galbraith et al.*, 2011; *Landschützer et al.*, 2015; *Le Quéré et al.*, 2007], implying that there may be an association with atmospheric CO_2. We do observe a relationship between ^{14}C and CO_2 but find the opposite to what we might expect at the end of the LIA chronozone; namely, reductions in the offset coincide with increases in atmospheric CO_2 as recorded in the West Antarctic Ice Sheet (WAIS) Divide ice core [*Bauska et al.*, 2015]

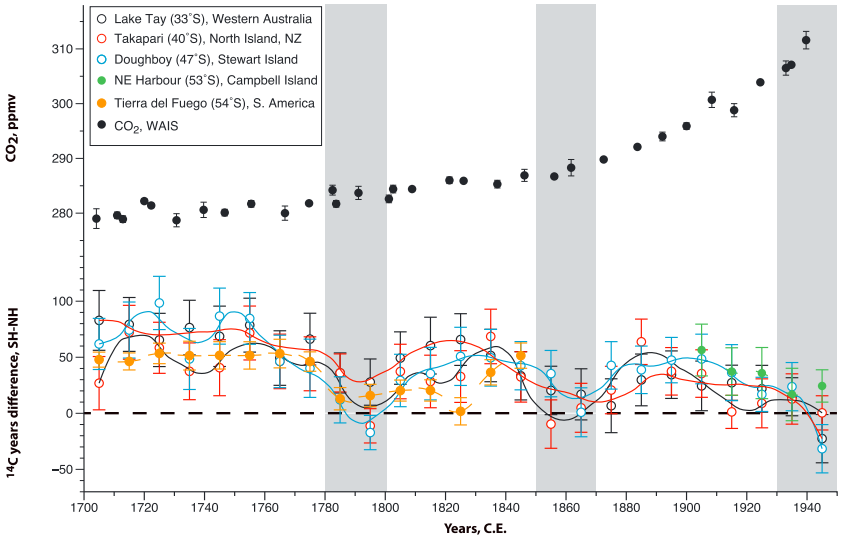

Figure 3. Decadal interhemispheric radiocarbon offsets calculated from the different tree ring series (colored circles) compared to the carbon dioxide (CO_2) concentration values (black solid circles) inferred from the West Antarctic Ice Sheet (WAIS) Divide ice core [*Bauska et al.*, 2015]; WAIS data are available at http://ncdc.noaa.gov/paleo/study/18316. A LOESS fit has been applied to each of the tree ring ^{14}C data sets. Gray columns denote common periods where the interhemispheric ^{14}C offset approaches zero, i.e., no offset between the hemispheres (dashed horizontal line).

(Figure 3). Curiously, the ^{14}C offset at the Tierra del Fuego site is less variable than at other sites, showing limited expression across the 1790 C.E. event.

It is intriguing that changes in Southern Ocean ^{14}C coincide with inflections in the CO_2 record. Our Southern Hemisphere radiocarbon values, however, strongly argue against a Southern Ocean source for the increase in atmospheric carbon dioxide. The collapse in the ^{14}C offset centered on 1790 C.E. coincides with a maxima in Northern Hemisphere radiocarbon ages (Figure 2) at the same time as the observed global increase in atmospheric CO_2 [*Ahn et al*., 2012] (Figure 3). While anthropogenic changes across Northern Hemisphere landscapes have been proposed as a possible cause for the rise in CO_2 at the end of the LIA [*Kaplan*, 2015] it seems unlikely that the near-modern ^{14}C values from carbon released from this source would be sufficient to drive the collapse in the observed interhemispheric offset [*Bauska et al*., 2015; *Graven*, 2015]. The reduced offset centered on 1790 C.E. is more consistent with an old-carbon (^{14}C-depleted) high-latitude terrestrial source, such as decaying peat [*Bauska et al*., 2015]. However, no substantive change in Northern Hemisphere ^{14}C is recorded across 1860 C.E., with relatively young ages across this period (Figure 2). Importantly, paleoreconstructions indicate that alongside a warming climate post-LIA [*PAGES 2 k Consortium*, 2013], there were highly variable changes in westerly airflow across the midlatitudes of the Southern Hemisphere [*Lamy et al*., 2010; *McGlone et al*., 2010; *Turney et al*., 2016a, 2016b], suggesting that the Southern Ocean sea-air flux of $^{14}CO_2$ may play a role.

Alongside high-latitude Northern Hemisphere peatlands, the tropics have also been acknowledged as providing a possible source of carbon around the time of the LIA [*Bauska et al*., 2015]. The strongest response of carbon fluxes in the tropics over recent decades, however, is not directly due to temperature changes but circulation changes associated with the El Niño–Southern Oscillation (ENSO). During La Niña events and stronger trade winds, cloud cover has been observed to decline across the low latitudes, increasing solar irradiance (a limiting factor on forest net primary productivity in the equatorial tropics) and carbon sequestration, impacting global atmospheric CO_2 [*Cleveland et al*., 2015; *Nemani et al*., 2003]. ENSO is known to impact changes in interhemispheric atmospheric radiocarbon via two key regions. First, in the tropics, La Niña events drive an increased flux of ^{14}C- depleted CO_2-rich water into the atmosphere at low latitudes [*Feely et al*., 1999; *Sutton et al*., 2014] which, as a result of an equatorward migration of the Intertropical Convergence Zone, can decrease the interhemispheric radiocarbon difference [*Turney and Palmer*, 2007]. ENSO, however, is also known to have a significant influence on climate and oceanographic conditions over the high latitudes of the Southern Hemisphere [*Turner*, 2004].

Significant changes in Southern Ocean air-sea exchange of carbon have been reported over recent decades and are projected for the future [*Landschützer et al*., 2015; *Xue et al*., 2015; *Yuan*, 2004], linked to changes in the strength of westerly airflow and the balance between upwelling of ^{14}C-depleted Circumpolar Deep Water and temperature of surface waters [*Bernardello et al*., 2014; *de Lavergne et al*., 2014; *Landschützer et al*., 2015; *Majkut et al*., 2014]. During La Niña events, for instance, a poleward shift in the Polar Jet Stream (and associated surface westerly winds) in the South Pacific is associated with a low-pressure system in the Bellinghausen Sea and cooler surface waters as a result of increased Ekman transport across the midlatitudes [*Landschützer et al*., 2015; *Yuan*, 2004]; positive sea-ice feedbacks further enhance regional cooling during these times (with the opposite association in the Weddell Sea) [*Bertler et al*., 2004; *Latif et al*., 2013; *Yuan*, 2004], reducing the sea-air flux of $^{14}CO_2$ to the Southern Hemisphere atmosphere. Given this relationship, our results imply that there was a change in the pervasive ENSO state around ~1790 and 1860 C.E., with more La Niña-like events on multidecadal timescales, resulting in an poleward shift (or strengthening) of westerly winds across the South Pacific, reducing ocean ventilation across the region. This inference is consistent with reconstructed decreases in ENSO variance during these periods [*Li et al*., 2013]. If the South Pacific is indeed a major driver of changes in the "interhemispheric" gradient, it may explain the relatively low temporal variability of Chilean ^{14}C, with the Polar Jet Stream redirected north in the southeast Pacific, effectively bypassing Tierra del Fuego [*Yuan*, 2004].

4. Conclusions

Recent work has suggested the global increase in atmospheric CO_2 during the termination of the Little Ice Age was driven by enhanced decay of peatlands in the Northern Hemisphere. An alternative source of carbon may have been the Southern Ocean. Here we use a network of absolutely dated tree ring series from across the midlatitudes of the Southern Hemisphere to measure atmospheric radiocarbon as a proxy of upwelling of ^{14}C-depleted abyssal waters. We find coincident regional collapses in the ^{14}C offset to the Northern

Hemisphere for approximately 20 years centered on 1790, 1860, and possibly 1950 C.E. Reductions in the regional offset strongly argue against a Southern Ocean source for the increase in atmospheric carbon dioxide at the end of the Little Ice Age and are consistent with a Northern Hemisphere terrestrial source. While a pervasive periodicity has previously been reported for the offset between New Zealand and the Northern Hemisphere, here we recognize these changes occur across most of the Southern Hemisphere. Our results suggest that alongside the long-term increase in CO_2 post-LIA, multidecadal variability in the sea-air flux of carbon-rich (^{14}C-depleted) subsurface waters may have been modulated by the El Niño–Southern Oscillation (ENSO). We find that long-term variability is near constant over Tierra del Fuego (54°S), suggesting air masses are relatively well mixed. In marked contrast, Campbell Island lies at a comparable latitude (53°S) to Tierra del Fuego and exhibits the greatest ^{14}C offset, offering considerable potential for future work to detect changes in Southern Ocean upwelling and the global carbon cycle since 1950 C.E.

Acknowledgments

Part of this work was undertaken during the Australasian Antarctic Expedition 2013–2014. C.S.M.T., C.F., and P.G. acknowledge the support of the Australian Research Council (FL100100195, FT120100004, and DP130104156). We thank the New Zealand Department of Conservation for the permission to undertake sampling on Campbell and Stewart Islands (permit: 37687-FAU and National Permit SO-29897-FLO, Southland Application 1011/38). The data reported in this study are provided in Table 1 and also lodged on the National Oceanic and Atmospheric Administration Paleoclimatology Database (https://www.ncdc.noaa.gov/data-access/paleoclimatology-data). We thank the two anonymous reviewers for their constructive comments which improved the manuscript.

References

Ahn, J., E. J. Brook, L. Mitchell, J. Rosen, J. R. McConnell, K. Taylor, D. Etheridge, and M. Rubino (2012), Atmospheric CO_2 over the last 1000 years: A high-resolution record from the West Antarctic Ice Sheet (WAIS) Divide ice core, *Global Biogeochem. Cycles*, *26*, GB2027, doi:10.1029/2011GB004247.

Bauska, T. K., F. Joos, A. C. Mix, R. Roth, J. Ahn, and E. J. Brook (2015), Links between atmospheric carbon dioxide, the land carbon reservoir and climate over the past millennium, *Nat. Geosci.*, *8*(5), 383–387.

Bernardello, R., I. Marinov, J. B. Palter, E. D. Galbraith, and J. L. Sarmiento (2014), Impact of Weddell Sea deep convection on natural and anthropogenic carbon in a climate model, *Geophys. Res. Lett.*, *41*, 7262–7269, doi:10.1002/2014GL061313.

Bertler, N. A. N., P. J. Barrett, P. A. Mayewski, R. L. Fogt, K. J. Kreutz, and J. Shulmeister (2004), El Niño suppresses Antarctic warming, *Geophys. Res. Lett.*, *31*, L15207, doi:10.1029/2004GL020749.

Braziunas, T. F., I. Y. Fung, and M. Stuiver (1995), The preindustrial atmospheric $^{14}CO_2$ latitudinal gradient as related to exchanges among atmospheric, oceanic, and terrestrial reservoirs, *Global Biogeochem. Cycles*, *9*(4), 565–584.

Briffa, K. R., and P. D. Jones (1990), Basic chronology statistics and assessment, in *Methods of Dendrochronology: Applications in the Environmental Sciences*, edited by E. R. Cook and L. A. Kairiukstis, pp. 137–152, Kluwer Acad., Norwell, Mass.

Bronk Ramsey, C., and S. Lee (2013), Recent and planned developments of the program OxCal, *Radiocarbon*, *55*(2–3), 720–730.

Bronk Ramsey, C., M. W. Dee, J. M. Rowland, T. F. G. Higham, S. A. Harris, F. A. Brock, A. Quiles, E. M. Wild, E. S. Marcus, and A. J. Shortland (2010), Radiocarbon-based chronology for Dynastic Egypt, *Science*, *328*(5985), 1554–1557.

Cleveland, C. C., P. Taylor, K. D. Chadwick, K. Dahlin, C. E. Doughty, Y. Malhi, W. K. Smith, B. W. Sullivan, W. R. Wieder, and A. R. Townsend (2015), A comparison of plot-based satellite and Earth system model estimates of tropical forest net primary production, *Global Biogeochem. Cycles*, *29*, 626–644, doi:10.1002/2014GB005022.

Collins, M., et al. (2013), Long-term climate change: Projections, commitments and irreversibility, in *Climate Change 2013: The Physical Science Basis. Contribution of Working Group I to the Fifth Assessment Report of the Intergovernmental Panel on Climate Change*, edited by T. F. Stocker et al., Cambridge Univ. Press, Cambridge, U. K.

Cox, P. M., and C. Jones (2008), Illuminating the modern dance of climate and CO_2, *Science*, *321*, 1642–1643.

Cox, P. M., R. A. Betts, C. D. Jones, S. A. Spall, and I. J. Totterdell (2000), Acceleration of global warming due to carbon-cycle feedbacks in a coupled climate model, *Nature*, *408*, 184–187.

Cullen, L. E., and P. F. Grierson (2009), Multi-decadal scale variability in autumn-winter rainfall in south-western Australia since 1655 AD as reconstructed from tree rings of Callitris columellaris, *Clim. Dyn.*, *33*, 433–444.

Currie, K., G. Brailsford, S. Nichol, A. Gomez, R. Sparks, K. Lassey, and K. Riedel (2011), Tropospheric $^{14}CO_2$ at Wellington, New Zealand: The world's longest record, *Biogeochemistry*, *104*(1–3), 5–22.

de Lavergne, C., J. B. Palter, E. D. Galbraith, R. Bernardello, and I. Marinov (2014), Cessation of deep convection in the open Southern Ocean under anthropogenic climate change, *Nat. Clim. Change*, *4*(4), 278–282.

Etheridge, D. M., L. P. Steele, R. L. Langenfelds, R. J. Francey, J. M. Barnola, and V. I. Morgan (1996), Natural and anthropogenic changes in atmospheric CO_2 over the last 1000 years from air in Antarctic ice and firn, *J. Geophys. Res.*, *101*(D2), 4115–4128.

Feely, R. A., R. Wanninkhof, T. Takahashi, and P. Tans (1999), Influence of El Nino on the equatorial Pacific contribution to atmospheric CO_2 accumulation, *Nature*, *398*(6728), 597–601.

Friedlingstein, P., M. Meinshausen, V. K. Arora, C. D. Jones, A. Anav, S. K. Liddicoat, and R. Knutti (2013), Uncertainties in CMIP5 climate projections due to carbon cycle feedbacks, *J. Clim.*, *27*(2), 511–526.

Galbraith, E. D., et al. (2011), Climate variability and radiocarbon in the CM2Mc Earth system model, *J. Clim.*, *24*(16), 4230–4254.

Graven, H. D. (2015), Impact of fossil fuel emissions on atmospheric radiocarbon and various applications of radiocarbon over this century, *Proc. Natl. Acad. Sci. U. S. A.*, *112*(31), 9542–9545.

Gregory, J. M., C. D. Jones, P. Cadule, and P. Friedlingstein (2009), Quantifying carbon cycle feedbacks, *J. Clim.*, *22*(19), 5232–5250.

Hogg, A. G., F. G. McCormac, T. F. G. Higham, P. J. Reimer, M. G. L. Baillie, and J. G. Palmer (2002), High-precision radiocarbon measurements of contemporaneous tree-ring dated wood from the British Isles and New Zealand: AD 1850–950, *Radiocarbon*, *44*, 633–640.

Hogg, A. G., L. K. Fifield, C. S. M. Turney, J. G. Palmer, R. Galbraith, and M. G. K. Baillie (2006), Dating ancient wood by high sensitivity liquid scintillation spectroscopy and accelerator mass spectrometry—Pushing the boundaries, *Quat. Geochronol.*, *1*, 241–248.

Hogg, A. G., J. Palmer, G. Boswijk, and C. Turney (2011), High-precision radiocarbon measurements of the tree-ring dated wood from New Zealand: 200 BC–AD 950, *Radiocarbon*, *53*(3), 529–542.

Hogg, A. G., et al. (2013), SHCal13 Southern Hemisphere calibration, 0–50,000 years cal BP, *Radiocarbon*, *55*(4), 1889–1903.

Hua, Q., M. Barbetti, and A. Z. Rakowski (2013), Atmospheric radiocarbon for the period 1950–2010, *Radiocarbon*, *55*(4), 2059–2072.

Kaplan, J. O. (2015), Holocene carbon cycle: Climate or humans?, *Nat. Geosci.*, *8*(5), 335–336.

Lamy, F., R. Kilian, H. W. Arz, J.-P. Francois, J. Kaiser, M. Prange, and T. Steinke (2010), Holocene changes in the position and intensity of the southern westerly wind belt, *Nat. Geosci.*, *3*(10), 695–699.

Landschützer, P., et al. (2015), The reinvigoration of the Southern Ocean carbon sink, *Science*, *349*(6253), 1221–1224.

Latif, M., T. Martin, and W. Park (2013), Southern Ocean sector centennial climate variability and recent decadal trends, *J. Clim.*, *26*(19), 7767–7782.

Le Quéré, C., et al. (2007), Saturation of the Southern Ocean CO_2 sink due to recent climate change, *Science*, *316*, 1735–1738.
Le Quéré, C., et al. (2009), Trends in the sources and sinks of carbon dioxide, *Nat. Geosci.*, *2*(12), 831–836.
Li, J., et al. (2013), El Niño modulations over the past seven centuries, *Nat. Clim. Change*, *3*, 822–826.
Majkut, J. D., J. L. Sarmiento, and K. B. Rodgers (2014), A growing oceanic carbon uptake: Results from an inversion study of surface pCO_2 data, *Global Biogeochem. Cycles*, *28*, 335–351, doi:10.1002/2013GB004585.
Mann, M. E., Z. Zhang, S. Rutherford, R. S. Bradley, M. K. Hughes, D. Shindell, C. Ammann, G. Faluvegi, and F. Ni (2009), Global signatures and dynamical origins of the Little Ice Age and Medieval Climate Anomaly, *Science*, *326*, 1256–1260.
Manning, S. W., B. Kromer, P. I. Kuniholm, and M. W. Newton (2001), Anatolian tree rings and a new chronology for the east Mediterranean Bronze-Iron ages, *Science*, *294*, 2532–2535.
Marshall, J., and K. Speer (2012), Closure of the meridional overturning circulation through Southern Ocean upwelling, *Nat. Geosci.*, *5*(3), 171–180.
McCormac, F. G., et al. (1998), Temporal variation in the interhemispheric ^{14}C offset, *Geophys. Res. Lett.*, *25*, 1321–1324.
McCormac, F. G., P. J. Reimer, A. G. Hogg, T. F. G. Higham, M. G. L. Baillie, J. Palmer, and M. Stuiver (2002), Calibration of the radiocarbon time scale for the Southern Hemisphere: AD 1850–950, *Radiocarbon*, *44*, 641–651.
McGlone, M. S., C. S. M. Turney, J. M. Wilmshurst, and K. Pahnke (2010), Divergent trends in land and ocean temperature in the Southern Ocean over the past 18,000 years, *Nat. Geosci.*, *3*, 622–626.
Meinshausen, M., T. Wigley, and S. Raper (2011), Emulating atmosphere-ocean and carbon cycle models with a simpler model, MAGICC6—Part 2: Applications, *Atmos. Chem. Phys.*, *11*(4), 1457–1471.
Nemani, R. R., C. D. Keeling, H. Hashimoto, W. M. Jolly, S. C. Piper, C. J. Tucker, R. B. Myneni, and S. W. Running (2003), Climate-driven increases in global terrestrial Net Primary Production from 1982 to 1999, *Science*, *300*(5625), 1560–1563.
PAGES 2 k Consortium (2013), Continental-scale temperature variability during the past two millennia, *Nat. Geosci.*, *6*(5), 339–346.
Reimer, P. J., et al. (2013), IntCal13 and Marine13 radiocarbon age calibration curves 0–50,000 years cal BP, *Radiocarbon*, *55*(4), 1869–1887.
Rodgers, K. B., et al. (2011), Interhemispheric gradient of atmospheric radiocarbon reveals natural variability of Southern Ocean winds, *Clim. Past*, *7*(4), 1123–1138.
Rubino, M., et al. (2013), A revised 1000 year atmospheric $\delta^{13}C$-CO_2 record from Law Dome and South Pole, Antarctica, *J. Geophys. Res. Atmos.*, *118*, 8482–8499, doi:10.1002/jgrd.50668.
Séférian, R., D. Iudicone, L. Bopp, T. Roy, and G. Madec (2012), Water mass analysis of effect of climate change on air–sea CO_2 fluxes: The Southern Ocean, *J. Clim.*, *25*(11), 3894–3908.
Stuiver, M., and T. F. Braziunas (1998), Anthropogenic and solar components of hemispheric ^{14}C, *Geophys. Res. Lett.*, *25*(3), 329–332.
Sutton, A. J., R. A. Feely, C. L. Sabine, M. J. McPhaden, T. Takahashi, F. P. Chavez, G. E. Friederich, and J. T. Mathis (2014), Natural variability and anthropogenic change in equatorial Pacific surface ocean pCO_2 and pH, *Global Biogeochem. Cycles*, *28*, 131–145, doi:10.1002/2013GB004679.
Trudinger, C. M., I. G. Enting, R. J. Francey, D. M. Etheridge, and P. J. Rayner (1999), Long-term variability in the global carbon cycle inferred from a high-precision CO_2 and $\delta^{13}C$ ice-core record, *Tellus*, *51B*, 233–248.
Turner, J. (2004), The El Niño–Southern Oscillation and Antarctica, *Int. J. Climatol.*, *24*, 1–31.
Turney, C. S. M., and J. Palmer (2007), Does the El Niño–Southern Oscillation control the interhemispheric radiocarbon offset?, *Quat. Res.*, *67*, 174–180.
Turney, C. S. M., R. T. Jones, C. Fogwill, J. Hatton, A. N. Williams, A. Hogg, Z. A. Thomas, J. Palmer, S. Mooney, and R. W. Reimer (2016a), A 250-year periodicity in Southern Hemisphere westerly winds over the last 2600 year, *Clim. Past*, *12*, 189–200, doi:10.5194/cp-12-189-2016.
Turney, C. S. M., et al. (2016b), Intensification of Southern Hemisphere westerly winds 2000-1000 years ago: Evidence from the subantarctic Campbell and Auckland Islands (52-50°S), *J. Quat. Sci.*, *31*, 12–19.
Xue, L., L. Gao, W.-J. Cai, W. Yu, and M. Wei (2015), Response of sea surface fugacity of CO_2 to the SAM shift south of Tasmania: Regional differences, *Geophys. Res. Lett.*, *42*, 3973–3979, doi:10.1002/2015GL063926.
Yuan, X. (2004), ENSO-related impacts on Antarctic sea ice: A synthesis of phenomenon and mechanisms, *Antarct. Sci.*, *16*(04), 415–425.